

# Extracting the critical rooting length in plant uprooting by flow from pullout experiments

# Extracting the critical rooting length in plant uprooting by flow from pullout experiments

**Valentina Bau'[1], Simone Zen[1], Giulio Calvani[2]and Paolo Perona[1]**

[1]Institute for Infrastructure and Environment, School of Engineering, The University of Edinburgh, Edinburgh, UK

[2]Department of Civil and Environmental Engineering, University of Florence, Florence, Italy

**Key Points:**

- We develop a free-body model to assess the critical rooting length of flexible plants from static pullout experiments.
- We validate the model on existing data from small-scale and field experiments.
- We assess the probability density function of time-to-uprooting for both datasets using a physically-based stochastic model.

Corresponding author: Valentina Bau', v.bau@ed.ac.uk

## Abstract

The growth and establishment of riparian vegetation on river bedforms is of hydrological as well as ecological importance as it helps in enhancing spatial heterogeneity and thus the biodiversity of river corridors. Yet, during floods, flow drag and scouring may reduce the rooting length of plants determining plant mortality via uprooting. In order for uprooting to occur, bed scouring must proceed until the rooting length reaches a critical value and drag forces exceed root residual anchorage. Therefore, the critical rooting length of a plant represents a crucial parameter to estimate the probability of plant removal due to flow erosion. However, difficulties in quantifying such length at the field scale have limited so far the performances of biomorphodynamic models for river bed evolution. In this work, we propose to assess the critical rooting length from controlled plant pullout experiments. To this aim, a free-body model of the forces acting on a flexible plant in a stream at different erosion stages is developed. At incipient uprooting, we conjecture that the root resistance at the critical rooting length equals that of a plant with equal rooting length when pulled out in static conditions. To illustrate our approach, we validate our model on three different datasets obtained from small- and real-scale plant uprooting experiments. A comparison between modelling and experimental observations reveals that the model provides valid results, despite its deterministic approach. The critical rooting lengths are finally used to assess the probability density function of the time-to-uprooting via a physically-based stochastic model.


## 1 Introduction

Riparian vegetation is strongly affected by river hydrology which promotes vegetation colonization and removal. Particularly, during high floods riparian plants are subject to strong mechanical stress that, combined with channel bed erosion, may lead to plant uprooting. The probability for a plant to successfully withstand a flood is essentially related to its root system [*Edmaier et al.*, 2011], which, besides a number of biological and ecological functions, [*Coutts*, 1983; *Waisel and Eshel*, 2002; *Gregory*, 2006] contributes to stabilize the plant. This results from sediment entanglement by root hairs, which increases the cohesion of soil and augments soil resistance to erosion [*Simon and Collison*, 2002; *Pollen and Simon*, 2005; *Pollen*, 2007], thus providing anchoring resistance [*Ennos*, 1989; *Ennos and Pellerin*, 2000; *Mickovski et al.*, 2007]. On the other hand, floods are also promoting plant recruitment through seeds and nutrients transport [*Mahoney and Rood*, 1998; *Johnson*, 2000].

Once established, riparian plants passively interact with river flow through their shape, density, and flexural rigidity [*Järvelä*, 2002; *Baptist et al.*, 2007; *Zong and Nepf*, 2011], altering scour and sedimentation processes [*Edwards et al.*, 1999; *Schnauder and Moggridge*, 2009]. By inducing deposition and stabilization of alluvial sediment, riparian vegetation acts as a river system engineer [*Gurnell*, 2013] in initiating pioneer island nuclei that develop in morphological structures and large-scale patterns [*Gregory and Atwell*, 1991; *Bertoldi et al.*, 2009; *Gurnell*, 2013; *Camporeale et al.*, 2013]. Thanks to this control exerted on morphological processes, riparian vegetation plays a key role in controlling streambanks and hillslopes erosion [*Pollen-Bankhead and Simon*, 2010], ultimately providing an important contribute to the ecotone heterogeneity [*Mahoney and Rood*, 1998; *Johnson*, 2000; *Camporeale et al.*, 2013] which sustains the biodiversity of riverine ecosystems. On the contrary, severe plants flood-induced mortality may trigger a process of habitat desegregation and biodiversity loss [*Lake et al.*, 2007; *Palmer et al.*, 2014] that negatively affect river physical restoration.

Plant uprooting by flow mostly occurs as a time-delayed process where drag forces as well as bed erosion processes contribute to reduce root anchoring. The minimum rooting length that allows plants to withstand uprooting is defined in the literature as critical rooting length, $L_c$ [*Perona et al.*, 2012; *Perona and Crouzy*, 2018]. Following such a mechanism, a plant is uprooted as soon as the critical rooting length is not enough to contrast the destabilizing forces acting on the above-ground biomass of the plant which now includes also the already exposed root. Laboratory and field experiments have demonstrated how the critical rooting length directly controls plant uprooting by flow [*Edmaier et al.*, 2015; *Calvani et al.*, 2019]. In their experiments *Edmaier et al.* [2015] and *Calvani et al.* [2019] estimated the time-to-uprooting by measuring the critical rooting length of plants, with a known total rooting length, subjected to a known erosion of the surrounding channel bed. Hence, the critical rooting length can be a relevant indicator to assess the percentage of biomass either uprooted or survived after a flooding event [*Perona and Crouzy*, 2018]. The stochastic model proposed by *Perona and Crouzy* [2018] is useful to calculate the probability density function of the time-to-uprooting once plant and river channel characteristics are assigned. However, the model requires to know the critical rooting length a priori.

Difficulties related to the spatial scale of erosion/sedimentation processes and to the recovery of plants after a flood make arduous to monitor vegetation response to flood disturbance and quantify its critical rooting length. In other experimental works the link between

the root resistance and the rooting length has been derived by means of plant pullout experiments at both the laboratory (e.g., [*Ennos*, 1989; *Bailey et al.*, 2002; *Mickovski et al.*, 2009; *Schwarz et al.*, 2011]) and the field scale (e.g., [*Karrenberg et al.*, 2003; *Tanaka and Yagisawa*, 2009; *Ying et al.*, 2011]). Despite laboratory measurements, no studies have been conducted to assess the critical rooting length associated to river hydraulics, morphology and vegetation properties. This represents an important problem that, if properly addressed, will provide insights into plant resistance and resilience to uprooting. Such result can be used to improve physically-based biomorphodynamics models, thus providing quantitative tools to support river restoration actions. Therefore the following question arises: how can the critical rooting length be assessed?

Considering that root resistance and rooting length are valuable inputs for revealing plants resilience to uprooting [*Edmaier et al.*, 2011, 2015; *Perona et al.*, 2012; *Bywater-Reyes et al.*, 2015], in this work, we show that the critical rooting length can be assessed from static uprooting experiments. A similar approach was initiated by *Bywater-Reyes et al.* [2015] and *Bankhead et al.* [2017], although an analytical expression for the critical rooting length was not derived. The present work uses the existing link between plant uprooting by flow and static uprooting experiments to develop a model for assessing the critical rooting length for variable erosion conditions, plant species and hydrology. In the model, the actions that contribute to plant uprooting by flow (hydrodynamics forces) are taken directly into account to balance the anchoring resistance of the root system by means of an equilibrium of forces.

This article is outlined as follows: in Section 2, the conceptual description and derivation of the model is presented together with the validation of the model on experimental data. Then, in Section 3, a comparison between experimental and modeled data is shown. Dataset is also casted under the probabilistic approach of *Perona and Crouzy* [2018] to compute the probability density function of the time-to-uprooting. Discussions and conclusions are presented in Section 4 and Section 5, respectively.

## 2 Modelling and datasets

### 2.1 Modelling the critical rooting length from static uprooting experiments

Plant uprooting by flow mostly occurs as a Type II uprooting mechanism [*Edmaier et al.*, 2011], which is a time-delayed process where drag forces as well as bed erosion pro-

cesses contribute to reduce root anchoring. At an initial time $t_0$, when bed erosion does not yet occur (Figure 1a), the forces acting on a submerged plant are reduced to the net buoyancy force $\mathbf{F_n}$ and the drag force $\mathbf{F_{d,n}}$. For plants with a low flexural rigidity [*Yagci et al.*, 2010; *Nepf*, 2012], the drag force progressively bends the portion of the plant above the ground until it lies parallel to the channel bed (Figure 1b). This horizontal reconfiguration of the plant was also adopted by *Calvani et al.* [2019]. At incipient uprooting, all the forces have to balance the resistance exerted by plant roots:

$$\mathbf{F_n} + \mathbf{F_{d,n}} + \mathbf{F_{d,t}} = \mathbf{R}. \tag{1}$$

where $\mathbf{F_n}$ is the net buoyancy force, $\mathbf{F_{d,n}}$ is the drag force, $\mathbf{F_{d,t}}$ is the friction action, and $\mathbf{R}$ represents the resistance exerted by the root system. The critical rooting length $L_c$ can be estimated through the equilibrium of forces in equation (1). In this configuration (Figure 1b) the plant is subject also to the friction force, $\mathbf{F_{d,t}}$, which, at the time-to-uprooting, concurs with the net buoyancy force and drag forces to plant uprooting, as expressed by equation (1). Plant flexibility allows us to interpret the physical configuration in Figure 1b as a pulley mechanism (Figure 1c) [*Calvani et al.*, 2019]. Therefore the vector sum of the destabilizing forces $\mathbf{F_n}$, $\mathbf{F_{d,n}}$, $\mathbf{F_{d,t}}$ is transmitted to the root system and to its mechanical resistance $\mathbf{R}$ regardless of the direction of the resultant force acting on the plant. However, root anchoring is particularly complex to obtain from first principles, given the unknown architecture of the soil-root system. In order to overcome such problem and quantify the root length resisting to the destabilizing forces at the time-to-uprooting, we can invoke experimental correlation laws linking the resistance force $\mathbf{R}$ and the total rooting length $L_t$ as derived from static pullout experiments. In pullout experiments $\mathbf{R}$ is generically expressed as follow:

$$\mathbf{R} = \mathbf{R}(L_t). \tag{2}$$

As a result, the vertical pullout force $\mathbf{F_p}$ balancing the root resistance at the incipient uprooting is directly related to the total rooting length $L_t$:

$$\mathbf{F_p} = \Phi(L_t). \tag{3}$$

where $\Phi$ is a fitting relationship extracted from experimental data. As the main rooting length $L_0$ was found to play a dominant role in the uprooting process for a given plant [*Edmaier et al.*, 2014], $L_t$ is then approximated to $L_0$, and equation (3) becomes a function of $L_0$ only:

$$\mathbf{F_p}(L_t) \approx \mathbf{F_p}(L_0). \tag{4}$$

The total resisting force exerted by the rooting length of a plant at incipient Type II uprooting, $\mathbf{R}$, can be compared to the force $\mathbf{F_p}$ that instantly pulls out the plant with an equal rooting length in static conditions. Under this assumption, the force balance expressed by equation (1) reads:

$$\mathbf{F_n} + \mathbf{F_{d,n}} + \mathbf{F_{d,t}} = \mathbf{F_p} \Longrightarrow \mathbf{F_p} = \mathbf{R}. \tag{5}$$

Hence, we assume that in the mechanism of uprooting of Type II the critical rooting length coincides with the main rooting length $L_0$ measured in static uprooting experiments (Figure 1d). Thus, the critical rooting length can be assessed as:

$$L_c \approx \Phi^{-1}(\mathbf{F_p} = \mathbf{R}) \tag{6}$$

where $\Phi^{-1}$ is the inverse function mapping $\mathbf{F_p}$ into $L_c$.

In order for the equivalence (5) to be valid, plant species, grain size distribution and soil saturated conditions are required to be the same for both scenarios (Figure 1b, 1d).

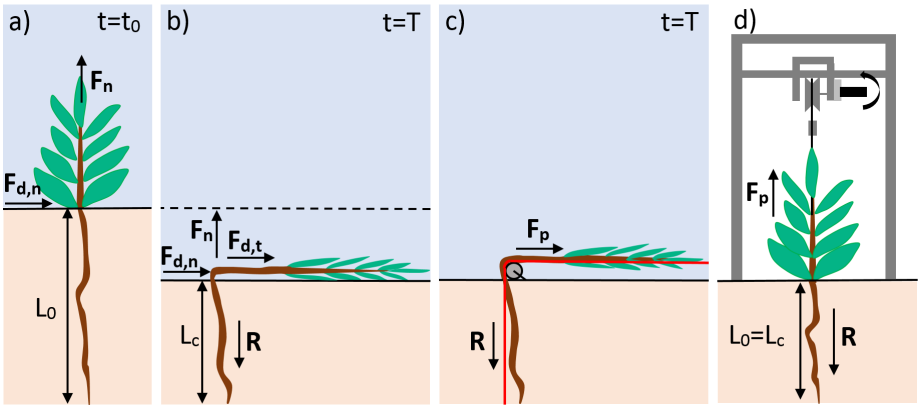


**Figure 1.** Outline of the free-body model and the force balance expressed in equation (5) a) Illustration of the forces acting on a upright seedling at an initial time $t$=$t_0$ without bed erosion conditions; b) Illustration of the forces acting on a bent seedling at uprooting time $T$; c) Schematic of a pulley mechanism for flexible plants, where the resultant destabilizing force $F_p$ is balanced by the resisting force $R$; d) Example of a schematic setup of vertical pullout experiments.

$\mathbf{F_{d,n}}$ is the normal drag force acting on the plant, $\mathbf{F_{d,t}}$ is the tangential drag force, $\mathbf{F_n}$ is the net buoyancy force, $L_c$ is the critical rooting length at time-to-uprooting and $L_0$ is the main rooting length of the plant when uprooted in static conditions. $L_c$ at incipient uprooting coincides with $L_0$ in static conditions.

Let us now explicit all the forces in equation (5). The flow exerts two drag forces: a normal drag force and a tangential drag force, respectively indicated with $\mathbf{F_{d,n}}$ and $\mathbf{F_{d,t}}$. $\mathbf{F_{d,n}}$ depends on the projected area of vegetation canopy on the flow direction $A_n$, the approaching flow velocity $u$ acting on the the vegetation element, the drag coefficient $C_D$ and the water density $\rho_w$. Its modulus is:

$$F_{d,n} = \frac{1}{2} C_D \rho_w u^2 A_n. \tag{7}$$

Similarly, the tangential drag force $\mathbf{F_{d,t}}$ depends on the surface area of the plant biomass exposed to the flow $A_t$ and the friction coefficient $C_f$. Its modulus can be expressed as:

$$F_{d,t} = \frac{1}{2} C_f \rho_w u^2 A_t. \tag{8}$$

In equations (7) and (8) the approaching velocity $u$ can be derived by using the value of the cross-section mean flow velocity or the local one as obtained from numerical simulations for more complex geometries. The flow resistance of vegetation is influenced by the type, density, shape and flexibility of the plant, the Reynolds number and the flow depth. Therefore, the drag coefficient $C_d$ is an empirical parameter that was approximated by Schlichting's formula (1962):

$$C_D = \begin{cases} \left(10^3/Re_D\right)^{0.25} & Re_D \leq 10^3 \\ \\ \min\left[0.976 + \left(\frac{10^{-3} Re_D^{-2}}{20.5}\right)^2 \, , \, 1.15\right] & 10^3 < Re_D < 4 \cdot 10^4 \end{cases} \tag{9}$$

where $Re_D$ is the obstacle Reynolds number calculated using the root diameter. The use of Schlichting's formula to compute $F_{d,n}$ is clearly an approximation that holds under the assumption (Figure 1b) that the only projected area on which $F_{d,n}$ acts is that of the root, whose shape can be easily approximated to a cylinder. In addition, the presence of leaves affects the friction coefficient $C_f$, which can result being from two to three times bigger than $C_d$ [*Järvelä*, 2002]. Accordingly, here, we assume $C_f$ to depend on the foliage.

The modulus of the net buoyancy force, $\mathbf{F_n}$ reads:

$$F_n = g(\rho_w - \rho_r)V_r + g(\rho_w - \rho_p)V_p + g(\rho_w - \rho_f)V_f \tag{10}$$

where $V_r$, $V_p$, $V_f$ are the the volumes of roots, stem and foliage, respectively; $g$ is the gravitational acceleration; $\rho_r$, $\rho_p$, $\rho_f$ are the density of roots, stem and foliage, respectively.

Considering plants with a very low flexural rigidity, the plant bends almost instantaneously towards the bed [*Aberle and Järvelä*, 2015; *Yagci et al.*, 2010]. Under these assumptions, the balancing equation (5) can be expressed as:

$$F_p(L_c) = \frac{1}{2}C_D\rho^* u^2 A_n + \frac{1}{2}C_f\rho^* u^2 A_t + g(\rho_w - \rho_r)V_r + g(\rho_w - \rho_p)V_p + g(\rho_w - \rho_f)V_f \tag{11}$$

As water and sediment mixture investing the plant have an actual density higher that that of clean water, $\rho_w$ has been replaced with a modified density term $\rho^*$:

$$\rho^* = \rho_g \left(\frac{V_g}{V_g + V_w}\right) + \rho_w \left(\frac{V_w}{V_g + V_w}\right), \tag{12}$$

where $\rho_g$ and $V_g$ are the density and volume of the sediment being moved, respectively. To complete the formulation of the problem and obtain a relationship for the critical rooting length $L_c$, we express the exposed rooting length, $L_e$, as a difference between the main rooting length, $L_0$, and the critical value, $L_c$,

$$L_e = L_0 - L_c. \tag{13}$$

$A_t$ from equation (8) can be decomposed in the following sum:

$$A_t = A_p + A_f + \pi n_r d_r L_e, \tag{14}$$

where $A_p$ is the surface area of the stem and $A_f$ is the surface area of the foliage. The third term is the surface area of the exposed root, whose shape can be approximated to a cylinder, $n_r$ is the number of the roots exposed to flow and $d_r$ the roots diameter.

The term $L_e$ also appears in one of the terms of equation (10): $g(\rho_w - \rho_r)V_r$, which has to be expressed as follow:

$$g(\rho_w - \rho_r)\pi n_r L_e \frac{d_r^2}{4} \tag{15}$$

Equation (11) finally reads:

$$\begin{aligned} F_p(L_c) = \frac{1}{2}C_D\rho^* u^2 A_n + \frac{1}{2}C_f\rho^* u^2 (A_p + A_f) + \frac{1}{2}C_f\rho^* u^2 \pi n_r d_r (L_0 - L_c) \\ + g(\rho_w - \rho_r)\pi n_r \frac{d_r^2}{4}(L_0 - L_c) + g(\rho_w - \rho_p)V_p + g(\rho_w - \rho_f)V_f. \end{aligned} \tag{16}$$

Equation (16) allows $L_c$ to be estimated once a relationship for the static uprooting force, $F_p$, is assigned. Notice that equation (16) is implicit in $L_c$ and would normally require an iterative numerical solution. However, for the particular case when the static uprooting

force can be expressed in a linear form, e.g, $F_p = kL_c$, (16) has the following relatively simple explicit solution:

$$L_c = \frac{\frac{1}{2}\rho^* u^2 \left(C_D A_n + C_f(A_p + A_f + \pi n_r d_r L_0)\right) + g\left((\rho_w - \rho_r)\pi n_r L_0 \frac{d_r^2}{4} + (\rho_w - \rho_p)V_p + (\rho_w - \rho_f)V_f\right)}{k + (\pi n_r d_r)\left(\frac{1}{2}C_f \rho^* u^2 + g\frac{d_r}{4}(\rho_w - \rho_r)\right)} \tag{17}$$

Finally, the proposed model has been validated by using the existing data available in the literature and presented in the subsections below.

## 2.2 Data source

### *2.2.1 Laboratory experiments*

Data of plant uprooting by flow are available from the laboratory experiments conducted by *Edmaier et al.* [2015] and *Calvani et al.* [2019]. Both experiments presented a similar set-up with plants placed in an erodible channel bed. The experimental runs were conducted with living seedlings of *Avena sativa*, chosen for their simple root structure and small stem size. Plants were cultivated outside the flume in plastic boxes with the particularity that the walls could be removed from the bottom. Hence, when seedlings had grown for required time, boxes could be placed into the flume bed and the lateral walls could be removed. Each plant was positioned at a certain distance from the neighbours to avoid root-root interactions which would lead to a relevant alteration of the root properties (e.g., root length density, radial spread, root distribution over density [*Smit et al.*, 2013]). Moreover, during the experiments a movable downstream wall was lowered at a constant rate $\dot{\eta}$, which was maintained equal to the erosion rate of the channel bed to obtain a quasi-parallel bed erosion. The experimental runs were conducted with living seedlings of *Avena sativa*, chosen for their simple root structure and small stem size. The scale of the experiments allowed the authors to record the time after which each plant was uprooted, the erosion depth, the amount of root exposed to the flow, and thus the computation of the critical rooting length. More details about the experimental conditions (e.g., number of samples tested, plant spatial arrangements) and the parameters available from Edmaier et al.'s and Calvani et al.'s datasets can be found in Table 1. The simple root architecture of *Avena sativa* seedling (Figure 2a) allowed the geometrical parameters of the free-body model to be estimated (equation (16)). In particular, by decomposing the seed into simple geometric shapes, whose characteristics and area are illustrated in Figure 2b, we estimated the volume of seed, grass and roots, as well as the projected and surface areas of the plant. As the stage of growth of the samples does not

have a relevant influence on the diameter of the roots and on the size of the seedling, we set the diameter of the roots and the size of the seed to constant values. Roots are approximated by cylinders with an average diameter, $d_r$, of 6mm. We assume a conic shape for the leaf because when plants are exposed to high velocities, the leaves rolled and reconfigured into cones [*Järvelä*, 2002]. With respect to the value of $C_d$, we used the formulation (9), whereas $C_f$ has two different values: 0.6 for leafless seedlings and 1 for seedlings with leaf. Both values were calibrated on one of the four Edmaier et al.'s flow settings. ($\dot{\eta}$=0.0431 m/s), and then applied to the remaining ones and to the other available datasets. The corresponding approaching velocity was calculated using the normal flow approximation and the Manning formula. Because mutual interactions among distinct samples are neglected in the laboratory runs, equation (11) can be applied independently for each single sample within the experiments.

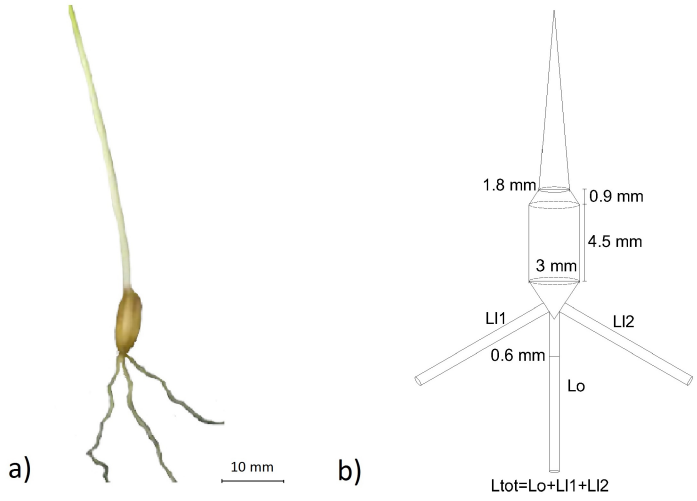


**Figure 2.** *Avena sativa* seedling and its model sketch. a) Morphology of a common *Avena sativa* seedling 4 days after seeding; b) The sketch of *Avena sativa* seedling and the different simple geometrical shapes used to approximate its morphology.

Static pullout data for *Avena sativa* are available from *Edmaier et al.* [2012, 2014] for different grain size distribution and saturation conditions. In order to validate equation (16) on Edmaier et al.'s dataset [*Edmaier et al.*, 2015] we refer to the curve of the maximum uprooting force from static pullout experiments obtained in *Edmaier et al.* [2014]. *Edmaier et al.* [2014] performed vertical uprooting experiments on *Avena sativa* species under different percentages of soil moisture content and grain size distribution. The static law to which

239 we refer is linear and was obtained for soil saturated conditions and for a grain size distribu-
240 tion equal to the one used in the flume experiments [*Edmaier et al.*, 2015].

$$F_p = kL_c \tag{18}$$

241 where $k$=2.1 and a goodness of fit $R^2$=0.40.

242 A different law needed to be used to validate the second dataset [*Calvani et al.*, 2019],
243 according to the grain size distribution of the flume bed. In this circumstance, we refer to the
244 uprooting law extrapolated by *Edmaier et al.* [2012] who run vertical uprooting experiments
245 on *Avena sativa* in fully saturated sediment conditions. Here the fitting relation is a second
246 degree polynomial equation, which reads to:

$$F_p = aL_c^2 + bL_c \tag{19}$$

247 where $a$=88.4 [N/m$^2$], $b$=0.65 [N/m] and a goodness of fit $R^2$=0.84.

248 In equation (18) and in equation (19) $F_p$ is expressed in [N] and $L_c$ is expressed in [m].
249 When $F_p$ is expressed in the same form of (18) and (19),equation (16) can be easily solved
250 without recurring to iterative methods.

251 ***2.2.2 Field experiments***

252 We refer to the dataset of *Bywater-Reyes et al.* [2015], who conducted lateral pullout
253 tests to measure the root resistance for two distinct pioneer woody seedlings species: *Pop-*
254 *ulus* and *Tamarix*. Their investigations were performed in three different river branches,
255 covering different river morphology, hydrological regimes and sediment size distribution.
256 Moreover, in order to assess how substrate scour may influence root resistance, the tests were
257 run for four different excavated scour depths, including 0.1, 0.2, 0.3 and 0.4 m (although the
258 last value was excluded from any statistical analysis because of the small number of sam-
259 ples available). Furthermore, floods with a recurrence time of two and ten years, $Q_2$ and $Q_{10}$
260 respectively, were measured and modeled to evaluate whether they would be sufficient to
261 uproot the species tested on the basis of their root resistance. In their work, *Bywater-Reyes*
262 *et al.* [2015] did not estimate the critical rooting length. Instead, they directly linked the
263 scour depth, which coincides with the exposed portion of root $L_e$, to the uprooting thresh-
264 old. Therefore, we used our model to assess $L_e$ (equation (20)) that corresponds to the scour
265 depth for which plant uprooting by flow occurs. The free-body model has been validated
266 against the dataset associated to the measurements conducted on the Bitterroot River, Mon-

tana, USA. The Bitterroot river is an unregulated gravel-bed river, with a drainage area of 6500 km$^2$ and an unregulated nivo-pluvial hydrological regime. The study bar contains only *Populus* seedlings. Plants for pull tests were selected randomly. The choice of this river was made according to some practical reasons: the highest number of pullout samples and the availability of enough streamflow hydrographs to provide an estimation of the averaged flow duration in movable bed condition. Hence, from equation (16) by using equation (13), we obtain:

$$L_e = \frac{F_p - \frac{1}{2}C_d\rho_w u^2 A_n - \frac{1}{2}C_f\rho_w u^2 A_s}{\frac{1}{2}C_f\rho_w u^2 \pi n_r d_r} \tag{20}$$

where $A_s$ is the surface area of the seedling exposed to the flow. As the shape of the samples can be approximated to a cylinder, the surface area is $A_s = \pi(HD)$. The product $(HD)$ is the frontal projection of the surface area of the upright plant $(A_{fr})$ of height $H$ and diameter $D$. When the plant is in contact with the sediment, the surface area subjected to the friction action of the flow is reduced. Therefore, assuming that the surface contact plant-sediment has an angle of approximately 120°, the effective exposed portion approaches 2/3 of the cylindrical surface area. Hence, the ratio between $A_s$ and $A_{fr}$ is the following expression: $\frac{A_s}{A_{fr}} = \frac{2}{3}\pi\frac{HD}{HD} \approx 2$. Therefore, in (20), $A_s \approx 2\ A_{fr}$, which is a quantity that is usually easily accessible also for complex plant canopies. The net buoyancy force is neglected and $\rho_w^*$ was set to the value of water density $\rho_w$ following *Bywater-Reyes et al.* [2015]. The approaching flow velocity has been modeled by *Bywater-Reyes et al.* [2015] through 1-D numerical simulations. The static uprooting laws were achieved by fitting the maximum pullout forces $F_p$ versus the frontal areas of the plants for a goodness of fit on average equal to 0.72. Overall, the fitting laws show that more force was needed to uproot plant with a lower $L_e$. Therefore the scour depth $L_e$ from each sample has been used to validate the model once the pullout forces, frontal area and basal diameter of the plants have been assigned. All the samples tested were divided into three classes according to the value of $L_e$ and part of the data were used to calibrate the friction coefficient, whereas the remaining part was used to test the model.

All the experimental conditions and the parameters available for the case of the Bitterroot River are illustrated in the third last column of Table 1.

Table 1: Summary table containing the experimental conditions and the parameters available for every dataset used to validate the free-body model.

| | *Edmaier et al.*[2015] | *Calvani et al.*[2019] | *Bywater-Reyes et al.*[2015] |
|---|---|---|---|
| plant species | *Avena sativa* | *Avena sativa* | *Populus* |
| plant growth conditions | laboratory | laboratory | outdoor (not monitored) |
| cultivation time/plant age | 48-110 hours | 96-144 hours | 1-5 years old |
| type of sediment | quartz sand | graded quartz sand | coarse gravel |
| $d_{50}$ | 1.35 mm | 0.57 mm | 23 mm |
| soil moisture | saturated | saturated | saturated |
| type of uprooting | by flow | by flow | pull test |
| uprooting location | artificial flume<br>2 m long, 0.3 m wide | artificial flume<br>5 m long, 0.44 m wide | Bitterroot River<br>river section width: 250 m |
| number of samples | 277 seeldings | 87 seedlings | 101 seedlings |
| temperature/climate | 22.5 – 26°C | 18 – 21°C | dry subhumid |
| plant spatial arrangement | 1 rows of 6 plants<br>3 rows of 6 plants | 2 rows of 4 plants | random |
| parameters available | $L_0$, $L_e$, $L_c$ | $L_0$, $L_e$, $L_c$ | $L_e$, $L_t$ |
| | $T$ | $T$ | - |
| | 4 different $Q$ [$m^3$/s] | 4 different $Q$ [$m^3$/s] | $Q_2$ and $Q_{10}$ [$m^3$/s] |
| | 4 different $\dot{\eta}$ [mm/s] | unique $\dot{\eta}$ [mm/s] | - |
| | static uprooting law* | - | pullout forces |
| | * *Edmaier et al.* [2012,2014] | | |

### 2.3 The stochastic model for the time-to-uprooting

*Perona and Crouzy* [2018] formulated an analytical expression which is able to provide the probability density function (pdf) of the time-to-uprooting $p_\tau$. The entire formulation of $p_\tau$ is withheld but it can be found in *Perona and Crouzy* [2018]. In our case, assuming constant the randomness of the noise in the erosion process, $g_t$, and the erosion rate, $\dot{\eta}$, the pdf of the time-to-uprooting, $T$, reduces to an inverse Gaussian distribution:

$$p_\tau = \frac{L_e e^{-\frac{(L_e-\dot{\eta}T)^2}{4\frac{g_t T}{2}}}(g_t T/2)}{2\sqrt{\pi}(\frac{g_t T}{2})^{3/2}} \tag{21}$$

$L_e$ is given or can be easily assessed once the critical rooting length is determined. Hence, the analytical expression (21) was implemented on both laboratory and field experiments. Function $p_\tau$ was used in Edmaier et al.'s data and Calvani et al.'s data to observe how different flow discharges can impact the statistical uprooting time of a plant. The comparison between the theoretical cumulative distribution of the dimensionless time-to-uprooting and the empirical distribution for Calvani et al.'s data is also provided and can be compared to the one obtained by using Edmaier et al.'s data in *Perona and Crouzy* [2018]. As for the field experiments, $p_\tau$ was computed to obtain the probability density functions of the time-to-uprooting of the plant samples uprooted by *Bywater-Reyes et al.* [2015]. We want to assess the time-to-uprooting and the uprooting probability of the samples at different scour depths $L_e$ if the samples are subjected to the different flow discharges ($Q_2$ and $Q_{10}$) taken into account by *Bywater-Reyes et al.* [2015].

## 3 Results

### 3.1 Model validation on dataset from laboratory experiments

#### *3.1.1 Model validation on Edmaier et al.'s dataset*

The modeled critical rooting lengths were obtained by implementing equation (16) for every sample collected during the laboratory experiments for all the flow settings. The static pullout relationship $F_p(L_c)$ that is required to solve equation (16) is given by equation (18). Such law appears suitable to compute the critical rooting length $L_c$ associated to all the experiments since it has been derived in similar environmental conditions, i.e., plants growing in fully saturated sediment which size ranges between 1 and 1.7 mm.

Figure 3 shows the comparison between measured (filled circles) and modeled (empty circles) critical rooting length $L_c$ for different values of the main rooting length $L_0$, for all

the samples and flow settings available. The model preserves the physical link between $L_c$ and $L_0$ observed at the laboratory scale. Moreover, the Pearson correlation coefficient, $r^2$, associated to the regression line within the panels of Figure 3 shows a higher value for the modeled values, $r^2$=0.99, than the measured ones for which $r^2$ assumes the values 0.68, 0.77, 0.87, and 0.89 respectively. This is essentially due to the simplified description of the size of the leaf introduced within the model that partially ignores the biological heterogeneity that characterized the laboratory runs. As the leaves were not measured during the experiments, indeed, existing correlations between the below- and above-ground biomass of *Avena sativa* seedlings have been used [*Edmaier*, 2014]. As a consequence, plants presenting same main rooting length $L_0$ are modeled with leaves of equal size. This simplification leads to a noticeable overlap of the modeled critical rooting length values $L_c$ when samples present equal value of $L_0$. All these observations highlight the intrinsic deterministic nature of the model that links $L_c$ to $L_0$.

For the sake of completeness, Figure 4 shows the correlation between the experimental values of $L_c$ found by *Edmaier et al.* [2015] and the ones obtained by implementing equation (16). The graph was obtained considering all the $L_c$ regardless of the flow setting. The high value of the Pearson coefficient ($r^2$=0.81) leads us to notice that the free-body model is able to provide a good approximation of the data observed experimentally.

#### *3.1.2 Model validation on Calvani et al.'s dataset*

In Calvani et al.'s dataset, the modeled critical rooting lengths were calculated from a different static uprooting law (Equation (19)). However, before solving equation (16) and comparing modeled and experimental data, an outlier removal method was applied to the dataset. Calvani et al.'s dataset shows some outliers, which may be the result of root-root interactions which are not accounted for in the present free-body model. In order to detect the outliers without constraining the dataset too much, we proceeded as follows. The outlier detection method was performed by imposing a threshold value of $3\sigma_L$ to the data (i.e., $\pm 1.5\sigma_L$). The value of the standard deviation $\sigma_L$ was extracted from Edmaier et al.'s data using those values of $L_c$ whose respective $L_0$ vary in a range of 20-25 mm for an erosion rate $\dot{\eta}$=0.058 mm/s (Figure 3b) [*Edmaier et al.*, 2015]. This specific flow setting shows the highest data variability ($r^2$=0.68) compared to the rest of the panels (Figure 3a, 3c, 3d). Hence, we discarded the values of $L_c$ observed by *Calvani et al.* [2019] that fell outside of the confidence interval $\pm 1.5\sigma_L$. The comparison between experimental and modeled crit-

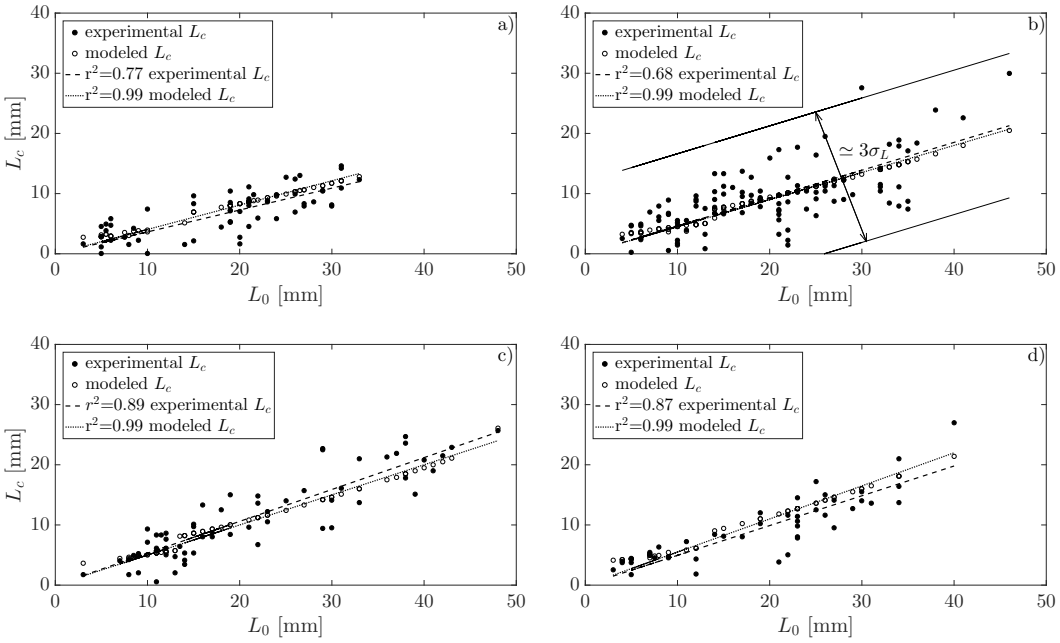


**Figure 3.** The panels represent the variation of the modeled (empty circles) and experimental (filled circle) critical rooting length $L_c$ with the main rooting length $L_0$ for the four flow settings considered by *Edmaier et al.* [2015]: a) $Q$=1.60 l/s and $\dot{\eta}$=0.0431 mm/s; b) $Q$=1.81 l/s and $\dot{\eta}$=0.058 mm/s; c) $Q$=1.94 l/s and $\dot{\eta}$=0.076 mm/s; d) $Q$=2.15 l/s and $\dot{\eta}$=0.1 mm/s.

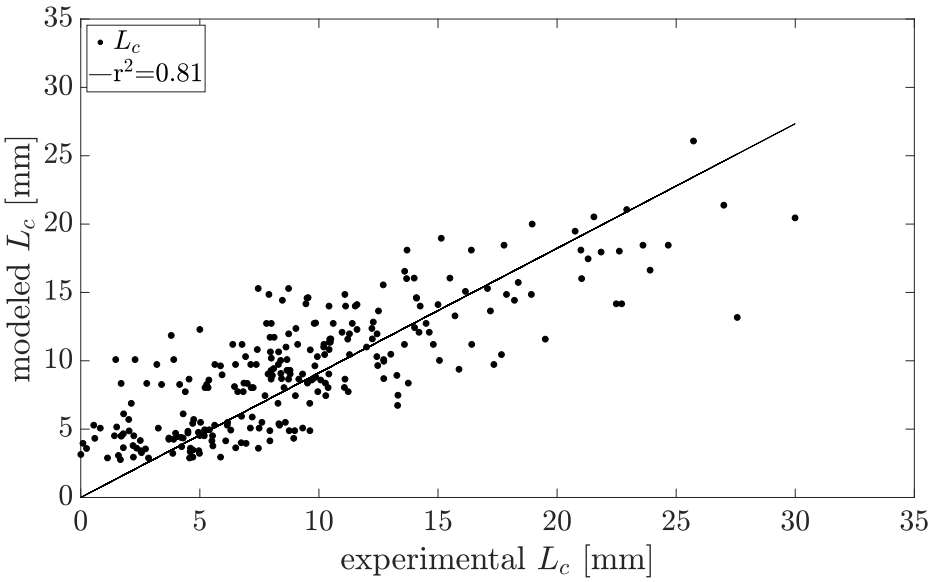


**Figure 4.** Regression plot between modeled and measured critical rooting lengths $L_c$ of the samples of *Avena sativa* seedlings tested by *Edmaier et al.* [2015] for all the four investigated flow settings.

ical rooting length $L_c$ for different values of main rooting length $L_0$ is reported in Figure 5a. Whereas, Figure 5b shows the correlation between the modeled and experimental critical rooting lengths $L_c$. The experimental data show a less strong correlation ($r^2$=0.42) between the main rooting length and its critical value compared to the previous dataset (Figure 3). Nevertheless, the regression line for the critical rooting length extracted from laboratory measurements is almost completely overlapped by the one obtained by fitting the values resulting from model application (Figure 5a). The latter result suggests that the model is able to preserve the inter-dependency between $L_c$ and $L_0$ as observed in the experimental data.

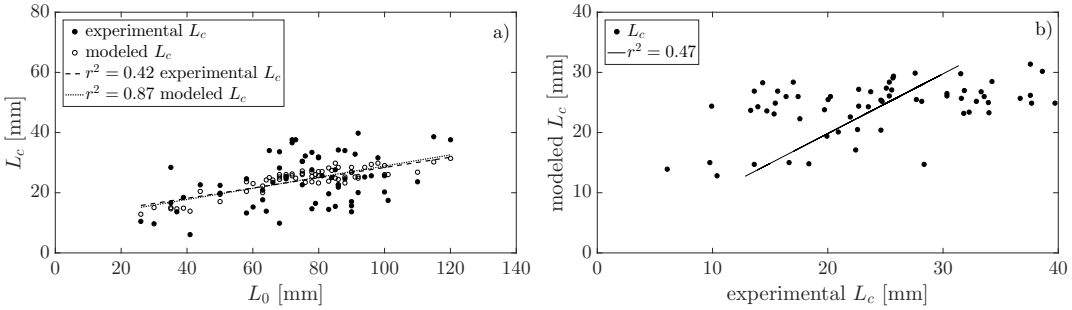


**Figure 5.** a) Variation of the modeled and experimental $L_c$ with $L_0$. The flow settings are not distinguished as the $\dot{\eta}$ is constant for every discharge analyzed; b) Modeled $L_c$ are plotted against experimental $L_c$.

### 3.2 Model validation on dataset from field experiments

The free-body model was applied to Bywater-Reyes et al.'s dataset referred to the field campaign carried out along the Bitterroot River on *Populus* species [*Bywater-Reyes et al.*, 2015]. In order to compute the scour depth through equation (20), a preliminary calibration procedure was required to determine the friction coefficient $C_f$ to be used to estimate the tangential component of the drag force and the tangential force acting on the exposed root portion. Figure 6a shows the results of the calibration procedure. A power law of the type $C_f = a * A_{fr}^b + c$ revealed to be the best approximation for the values of $C_f$ for the three different scour depths. The parameters $a$, $b$ and $c$ assume different values according to the entity of the scour $L_e$ considered and generate curves that reach almost an asymptotic-constant value for $A_{fr}$ greater than 0.06. As expected, the friction coefficient $C_f$ increases with $A_{fr}$. However, Figure 6a shows that for equal $A_f$, the values of $C_f$ decrease when $L_e$ grows. This result agrees with the intuitive concept for which a lower value of the friction force is needed

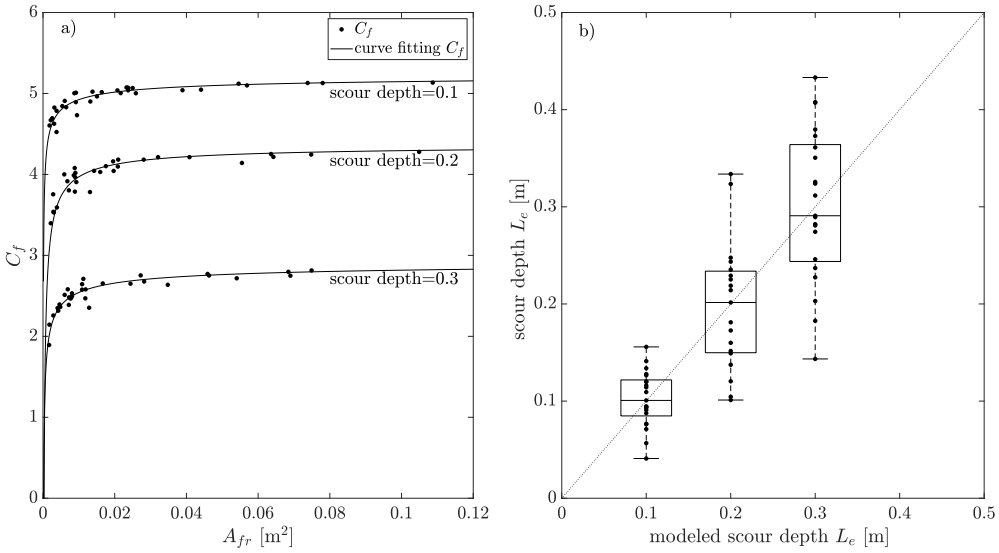


**Figure 6.** a) Power fitted curve used to find the law of variation of $C_f$ with $A_{fr}$ for the three different scour depths considered; b) The values of $L_e$ defined by *Bywater-Reyes et al.* [2015] are plotted against the modeled scour depths. Boxplots help to notice the degree of dispersion and skewness of the modeled data around the average.

to uproot a plant whose root system has lost part of its residual anchoring resistance due to the scouring developed around the plant [*Edmaier et al.*, 2011].

River geometry and hydraulics at the bar, where samples were collected during the field campaign, complete the input required to compute both drag and tangential forces. Figure 6b shows the regression between the values of the scour depths observed in the field and those modeled via equation (20). Differently from the application to the laboratory dataset, in this case the samples include several plant species that were recorded with similar scours. On the contrary, the free-body model returns different values of scour depths when changing plant characteristics. Therefore the comparison between modeled and observed scour depths are described trough a box plot, whereby the boxes including the modeled points are adjusted such that the average values of the modeled scour depth $L_e$ is set to coincide with that associated to the observed scour depth (Figure 6b).

401 ## 3.3 Probability distribution of the time-to-uprooting

402 ### *3.3.1 Laboratory experiments dataset*

403 The physically-based stochastic model for the time-to-uprooting proposed and vali-
404 dated on Edmaier et al.'s data by *Perona and Crouzy* [2018] is here implemented against the
405 plants uprooting times measured. The distribution of the uprooting times was obtained from
406 both experimental datasets for different values of the main rooting length $L_0$ and discharge
407 (Figure 7a and 7b). Because the model requires the variance of the time-to-uprooting as in-
408 put and time-to-uprooting was computed for every sample, its application was conducted for
409 a range of main rooting length $L_0$ rather than just one value. The range was kept as narrow
410 as possible to be close to the theoretical single value but including enough samples such that
411 to allow a significant variance to be computed. The probability distributions for the time-
412 to-uprooting $p_\tau$ for the different groups of samples collected in the laboratory runs are re-
413 ported in Figure 7a and 7b. In both figures $p_\tau$ are plotted against the dimensionless time-to-
414 uprooting: $T/\bar{T}$. where $\bar{T}$ is the averaged value of the uprooting time for every range of $L_0$.
415 Hence, we can estimate the influence of the flow rate on the uprooting time probability of
416 plants with similar rooting lengths. It is sufficient to compute $1 - \int_0^T p_\tau$ (the percentage of
417 biomass that survives the event) to realize that the random component is successfully inter-
418 preted by the model. For instance, in Figure 7b, plants with $L_0$=85-90mm have more chance
419 of surviving the event for a higher flow rate magnitude ($Q$=10.5 l/s). This means that the
420 level of noise is clearly high compared to the strength of the deterministic drift. The opposite
421 can be said for plants with $L_0$=28-30mm (Figure 7a), where the percentage of biomass that
422 survives is higher for the lowest value of flow ($Q$=1.96l/s). The result in this case is intuitive
423 and shows that for those ranges of values of $L_0$ the dynamics gets closer to the hypothetical
424 condition of a purely deterministic erosion process with no process noise. Higher discharges
425 shift the probability distribution toward right thus decrease the probability of plants to sur-
426 vive the flood with differences due to roots characteristics.

427 Figure 7 shows the good correspondence between the theoretical cumulative density
428 function of the time-to-uprooting, $P_\tau$, and the cumulative distribution associated to the data
429 extracted from the laboratory observations of *Calvani et al.* [2019]. The empirical curve is
430 well approximated by the theoretical one, except for a short mismatch that emerges when $P_\tau$
431 approaches to 1. The distribution shows a good agreement also with the data of Edmaier et
432 al.'s datasets (see *Perona and Crouzy* [2018]).

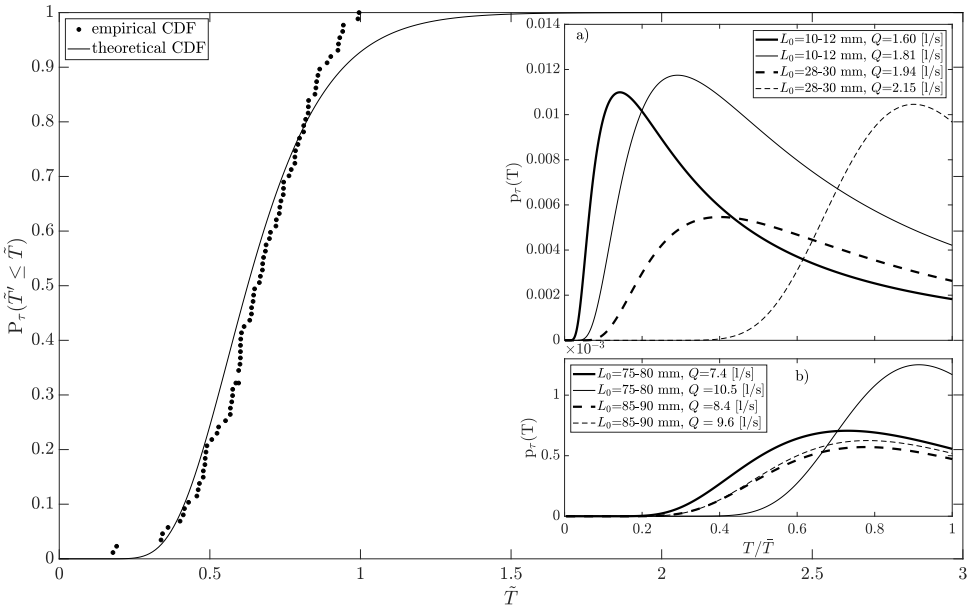


**Figure 7.** Comparison between the theoretical and the empirical (scatter plot) cumulative density functions of the dimensionless time-to-uprooting $\widetilde{T}$=$T\dot{\eta}/L_0$; Probability density functions of time-to-uprooting $p_\tau(T)$ for constant ranges of $L_0$, different flow rates $Q$, different magnitude of process variance and erosion velocity $\dot{\eta}$ for a) Edmaier et al.'s data [*Edmaier et al.*, 2015] ; b) Calvani et al.'s data [*Calvani et al.*, 2019].

### *3.3.2 Field experiments dataset*

It has been stated that the scour depths of the plants from the field experiments [*Bywater-Reyes et al.*, 2015] coincide with the exposed portion of root at incipient uprooting. Therefore, the distribution of the uprooting times (equation (21)) can also be computed for every group of samples (Figure 8). The variability for the $p_\tau$ was assessed by the variance of the values of the maximum pullout force within group of plants with equal scour depths $L_e$. Indeed, the variance of the uprooting force can be representative of the variability of the process for being indirectly linked to the time-to-uprooting. Moreover, differently from laboratory data, data from field experiments does not provide information on the vertical erosion rate of the channel bed $\dot{\eta}$. In order to estimate such rate we determined the total time for which water flow is able to rework the channel bed based on the Shields's definition of sediment mobility [*Shields*, 1936]. According to Shields's theory, in order for sediment to be mobilized, the shear stress at the bottom has to be greater than its critical value associated to the incipient sediment movement. Since both 2- and 10-years recurrence time discharges, $Q_2$ and $Q_{10}$ respectively, may be considered formative [*Doyle et al.*, 2005], values greater than

$Q_2$ and $Q_{10}$ are assumed to be able to induce morphological changes, i.e., scours within the channel bed. The bankfull Shields numbers relevant to $Q_2$ and $Q_{10}$ [*Bywater-Reyes et al.*, 2015] show that the Bitterroot is a threshold river [*Church*, 2006] where the limit for bed material transport is exceeded by a moderate amount. Thus, we measured the time when $Q > Q_2$ and $Q > Q_{10}$ over the historical flood series in order to compute the averaged duration of the flow erosion process $\hat{t}$ for the two dominant discharges (Figure 9). Within the available historical series, the number of events for which $Q > Q_2$ is 32 with an average value $\hat{t}$ of 73.6 hours and a standard deviation $\sigma_T$=72.7 hours, whereas the only event with $Q > Q_{10}$ has an average value, $\hat{t}$= 49.32 hours. Once information on the average time $\hat{t}$ and the average local scour $L_e$ were collected, the vertical erosion rate was computed as follows:

$$\dot{\eta} \approx \frac{L_e}{\hat{t}} \tag{22}$$

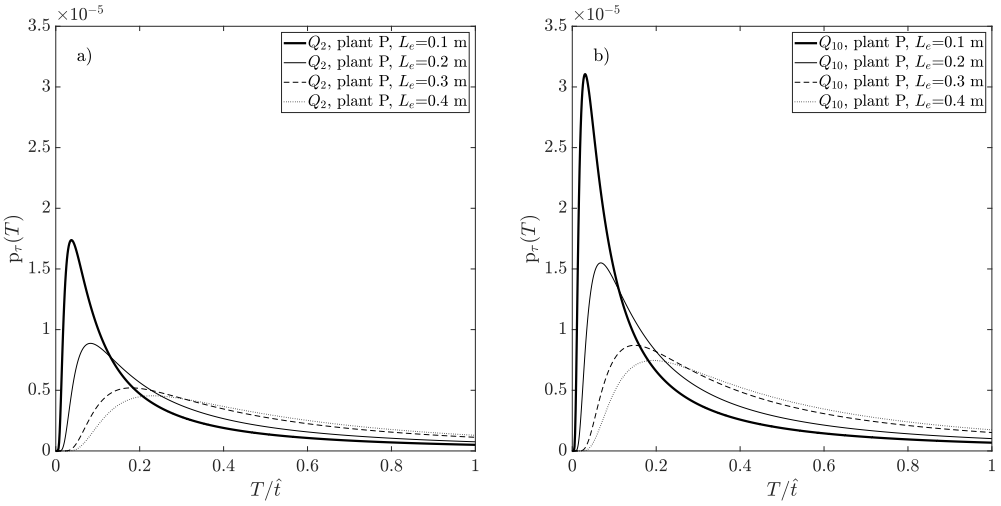


**Figure 8.** Probability density functions of time-to-uprooting $p_\tau(T)$ for Bitterroot river for *Populus* species for four different values of scour depths. a) flow rate $Q_2$; b) flow rate $Q_{10}$.

Figure 9 shows the probability density functions of time-to-uprooting for both the discharges $Q_2$ and $Q_{10}$ for different values of the scour depths $L_e$. The shapes of the distributions are very similar for both the flow rates when increasing $L_e$. However, the mode of the distributions shows remarkably different magnitudes, which clearly affects the probability of uprooting given by $\int_0^T p_\tau d\tau$ over equal time erosion intervals $(0, T)$. Furthermore, the scour depth $L_e$ exerts a fundamental control on the uprooting probability (Figure 10). The

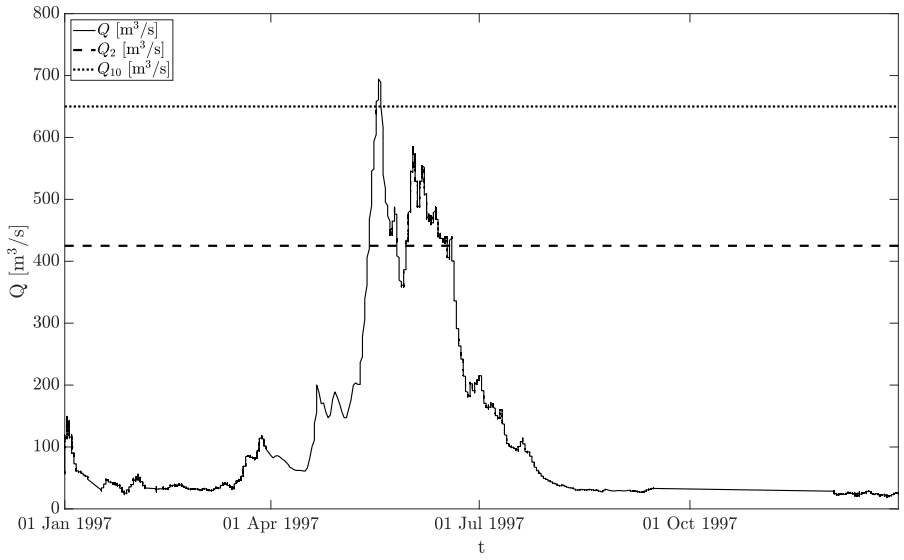


464 **Figure 9.** The hydrograph for the Bitterroot River, Montana, USA, in the year 1997. The flow rates $Q_2$
465 (dashed line) and $Q_{10}$ (dot line) provide a graphical representation of the amount of time over which the
466 riverbed is morphologically active.

476 observed trend emerges because constant values of flow rate are associated to constant drag
477 forces.

## 478 4 Discussion

479 The free-body model proposed in this work provided satisfactory results in determin-
480 ing the critical rooting length of riparian plants undergoing uprooting by flow. Despite the
481 assumptions introduced to tackle the problem analytically, the proposed model is able to pro-
482 vide an estimation of the critical rooting length even when applied to a real-scale case where
483 plants presents complex morphology (i.e., leaf shape and roots structure) and are exposed to
484 a real hydrograph [*Bywater-Reyes et al.*, 2015]. The analytical solution for the critical root-
485 ing length is easily obtained once the drag forces are determined and a static uprooting law
486 is assigned. However, the issue that makes uprooting difficult to frame is that the main root-
487 ing length $L_0$ is not known and it varies with species and age. Estimating the main rooting
488 length still remains a challenge. For certain species, the main rooting length was found to be
489 dependent on the stage of growth of the plant, on the intra e inter species variability [*Can-*
490 *non*, 1949; *Köstler et al.*, 1968] as well as on the spatial and seasonal variation [*Kiley and*

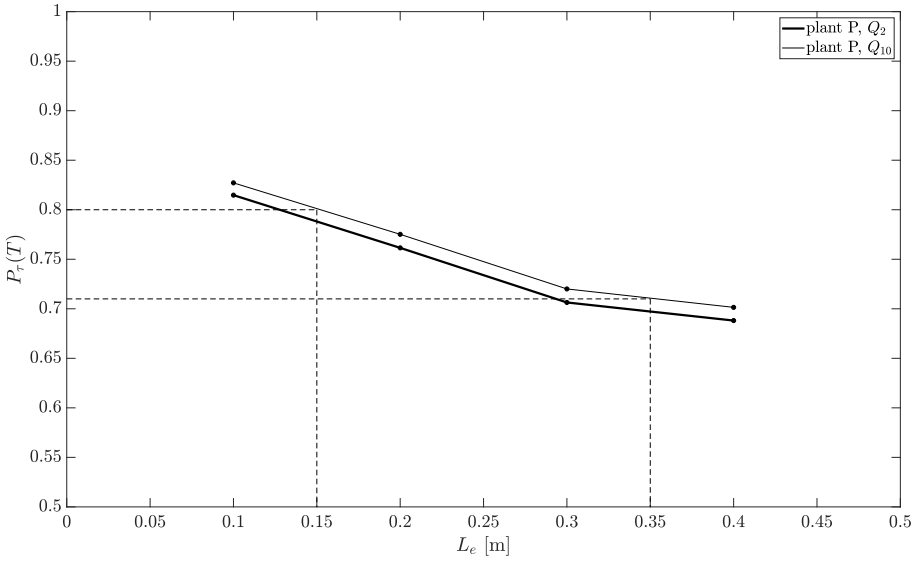


**Figure 10.** The uprooting probability in the Bitterroot river is plotted against the variation of scour depths for $Q_2$ and $Q_{10}$. $X_1$ and $X_2$ are two generic plants with two different scour depths $L_e(X_1)$=0.15 m and $L_e(X_2)$=0.35 m, respectively.

*Schneider*, 2005]. With increasing plant stem, the root system and the main rooting length increase in diameter and length [*Ennos*, 1993; *Waisel and Eshel*, 2002]. To a certain extent, prediction of the main rooting length from above-ground biomass measurements is, however, possible. In fact, for young *Avena sativa* seedlings (maximal 7-days-old seedlings) an estimation of the main rooting length was easily achieved by *Edmaier* [2014]. Generally, such types of correlation laws may be hard to obtain for older plant and with a more complicated morphological structure (see Calvani et al.'s dataset). In order to better understand the results and the generality of the approach used, the hypothesis and limitations of the model need to be examined. In particular, the assumptions made on the plant morphology, e.g., the approximation of the total root length with a single main root, and the assumption of the plant to be completely bent under the drag force are considered to be the strongest simplification introduced in the model. The latter hypothesis might not be suitable in real cases, since drag acting on a canopy usually changes with bending and exposure time [*Nepf*, 2012]. This can also explain the lower correlation ($r^2$=0.42) observed on Calvani et al.'s data between the main rooting length and its critical value in Figure 5a. This can be ascribed to a poor correlation between the above and below-ground biomass for plants in a relatively advanced stage of growth [*Pasquale et al.*, 2014]. As a matter of fact, the plants tested in the experimental

runs by *Calvani et al.* [2019] have rooting lengths which are twice as long as the ones tested by *Edmaier et al.* [2015]. On the contrary, Figure 5b shows that the model provides a weaker correlation between the experimental and modeled data ($r^2$=0.47) than the one that was obtained for Edmaier et al.'s data. This might be due to the inadequacy of the static uprooting law of equation (19) which was derived for plants with simple root architecture. In fact, the pullout law implemented in (16) was derived for data obtained by testing younger samples of *Avena sativa* [*Edmaier et al.*, 2014] in a sediment that was not exactly the one used by *Calvani et al.* [2019].

Accounting for the drag forces on a flexible plant, however, has revealed the influence of the shear force component, which is strongly affected by the value of the friction coefficient $C_f$. The difficulties of estimating a correct value for $C_f$ are mainly related to the flapping instability that may occur for plants with relatively long leaves. Such mechanism was found responsible to increase the turbulent wake and generate very marked spikes in the friction factor [*Connell and Yue*, 2007]. The degree of dispersion in the experimental data seems to be dependent, to some extents, on the flapping mechanism, and to the vibrations induced on the plant. The flapping instability together with local fluctuations of erosion-deposition processes are a source of noise that can lead uprooting to occur for different times even under the same initial conditions [*Perona and Crouzy*, 2018]. Randomness also emerges as a consequence of the load redistribution among sliding roots [*Crouzy and Perona*, 2012; *Edmaier et al.*, 2014] as well as from the readjustment of the portion of the soil that adheres directly to the roots when uprooting occurs. Hence, the intrinsic process noise is also enclosed in the hidden part of the plant, where tortuosity [*Schwarz et al.*, 2010], friction between sand grains and roots, and the strong non isotropic distribution of the strength over roots play a key role. All of these processes are not able to be taken into account by the free-body model here proposed and clearly contribute to its limits. Therefore, we applied the stochastic model proposed by *Perona and Crouzy* [2018] to study the influence of channel bed scour, water discharge and initial rooting length on plant uprooting probability.

The application of the analytical model [*Perona and Crouzy*, 2018] on Bywater et al.'s data produces an alternative and valid interpretation of the data compared to the one adopted by the authors [*Bywater-Reyes et al.*, 2015]. Figure 10 shows that, for a constant value of flow rate, plant uprooting probability decreases for increasing scour depths. At first glance, this outcome might be counterintuitive and requires a detailed explanation. For the sake of simplicity let us consider a flooding event of constant magnitude and assigned duration, T.

Two generic plants $X_1$ and $X_2$ (Figure 10) with the same total rooting length $L_0$ but requiring two different scour depth $L_e(X_1) < L_e(X_2)$ to uprooting, will result in two different uprooting probabilities. In order to uproot them, the stream has thus to "work" (i.e., scour) more for plant $X_2$ than for plant $X_1$, although $L_{c2} = L_0 - L_e(X_2) < L_{c1} = L_0 - L_e(X_1)$. Given that the flood has limited duration and that the erosion process has an inherent stochasticity, this results in a lower probability for the critical scour depth $L_e(X_2)$ is achieved and plant $X_2$ is uprooted (see *Perona and Crouzy* [2018] for details about the stochastic uprooting dynamics). Notice that this process is thus fundamentally different from imposing a scouring and let the stream to uproot the plant via drag forces only, which would lead to the same conclusion found by *Bywater-Reyes et al.* [2015].

Furthermore, it is interesting to study how the critical rooting length depends on the properties of the river channel rather than on a local portion of it. Figure 11 shows the variation of the critical rooting length, $L_c$, according to the stream power per unit width $w$ for different values of the main rooting length, $L_0$. The inset panel of Figure 11 shows the experimental values of *Edmaier et al.* [2015] and highlights how the critical rooting lengths are scattered around their relative averaged values for the four investigated flow settings. Notice that the four curves are truncated when the critical rooting length $L_c$ equals the averaged rooting lengths of the plants. Figure 12 reveals the trend of different values of $C_f$ for a fixed $L_0$ when varying $w$ and $L_c$. Here equation (17) was implemented by using the static law (18).

## 5 Conclusion

In this article, we derived a free-body model assessing the critical rooting length of plants on the basis of plant pullout experiments. The model was used to reproduce Type II uprooting mechanism by computing a force equilibrium between the residual root resistance and the normal and tangential drag forces exerted by flow processes.

The model has been validated against three different experimental datasets available in the literature both at the laboratory and field scale. The comparison between modeling results and experimental observations are satisfactory. Despite the simple hypothesis introduced, the model is able to predict the critical rooting length, once river and plants characteristics are assigned. This represents a crucial aspect since in real river channels the spatial and temporal scale of the process do not allow the critical rooting length to be directly recorded.

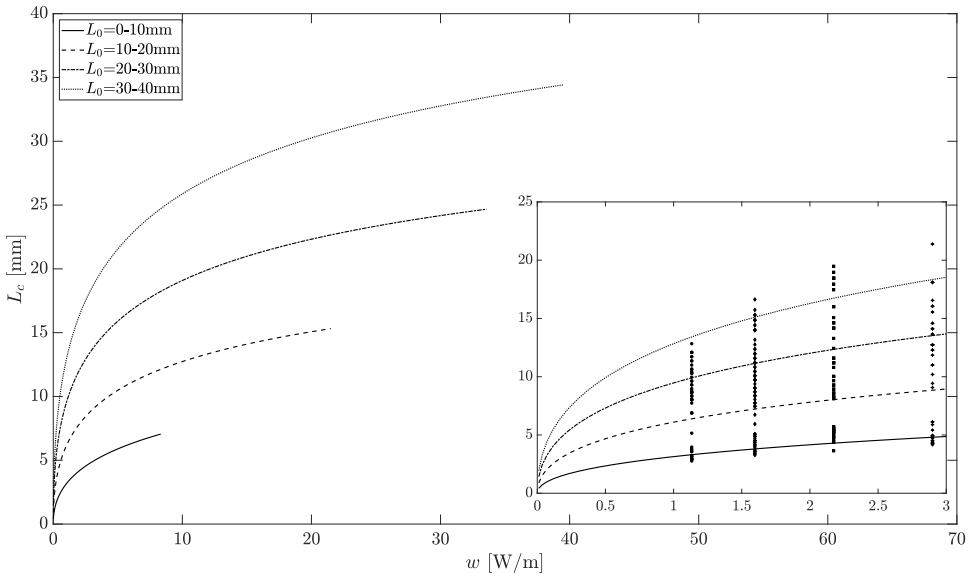


**Figure 11.** Variation of $L_c$ with stream power per unit width for four different ranges of $L_0$, for $F_p = 2.1L_c$. In the inset panel, the experimental values of *Edmaier et al.* [2015] are also reported.

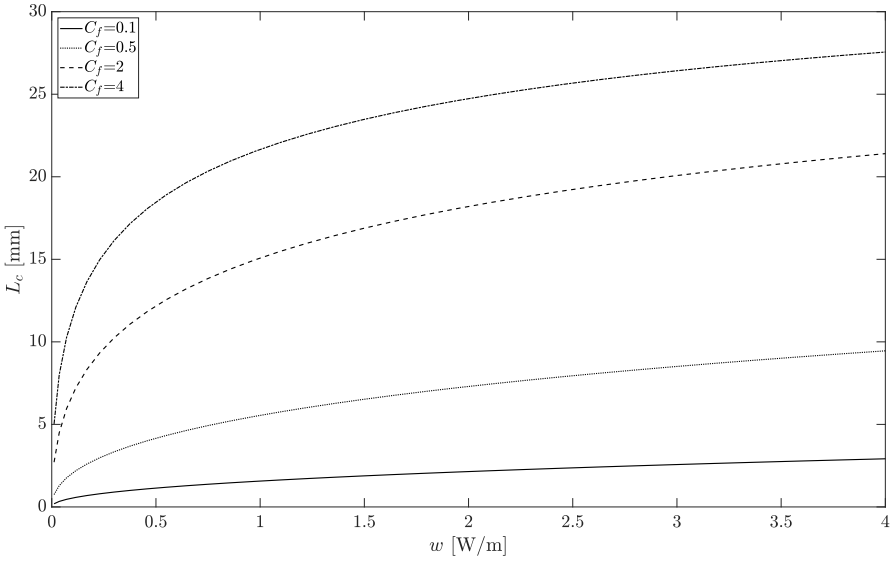


**Figure 12.** Variation of $L_c$ with the stream power per unit width for four different values of $C_f$, for $F_p = 2.1L_c$.

In addition, the stochastic model for time-to-uprooting has been applied in order to explore the influence of water discharge and scour depth on the uprooting process in terms of the percentage of plants that can survive or not to a flood.

We argued that an integration of the free-body model here proposed will further improve stochastic models of the type proposed by *Perona and Crouzy* [2018], by including the control exerted by the drag forces. Moreover, the critical rooting length will be computed from the characteristic of both river flow and plants rather than being assigned *a priori*.

Modelling the critical rooting length will provide insights into plant uprooting mechanism. This will help to improve numerical models that impose a value for the critical rooting length (e.g., *Caponi and Siviglia* [2018]) or models which adopt an uprooting threshold function of a modified critical Shield number [*Bertoldi et al.*, 2014; *Zen et al.*, 2016] or of a dose-response relationship [*Oorschot et al.*, 2016]. Modeling advances will, to the same extent, increase reliability on green engineering techniques applied to river management.

## A: Nomenclature

Table A.1: Nomenclature Used in the Paper.

| Symbol | Description | Unit |
|---|---|---|
| $A_f$ | surface area of the foliage | [$L^2$] |
| $A_{fr}$ | projected surface area of the upright plant | [$L^2$] |
| $A_n$ | drag exposed projected area | [$L^2$] |
| $A_p$ | surface area of the stem | [$L^2$] |
| $A_t$ | drag exposed surface area | [$L^2$] |
| $C_D$ | drag coefficient | [-] |
| $C_f$ | friction coefficient | [-] |
| $D$ | upright plant diameter | [L] |
| $d_r$ | root diameter | [L] |
| $F_{d,n}$ | drag force | [M· L· $T^{-2}$] |
| $F_{d,t}$ | friction force | [M· L· $T^{-2}$] |
| $F_n$ | net buoyancy force | [M· L· $T^{-2}$] |
| $g$ | gravitational acceleration | [M· $T^{-2}$] |
| $g_t$ | erosion process noise | [$L^2$·$T^{-1}$] |
| $H$ | upright plant height | [L] |
| $L_c$ | critical rooting length | [L] |
| $L_e$ | exposed rooting length | [L] |
| $L_0$ | main rooting length | [L] |
| $L_t$ | total rooting length | [L] |
| $n_r$ | number of roots | [-] |
| $p_\tau$ | pdf of the time-to-uprooting | [$T^{-1}$] |
| $P_\tau$ | uprooting probability | [-] |
| $Q$ | flow rate | [$L^3$· $T^{-1}$] |
| $Q_2$ | 2-years recurrence time discharge | [$L^3$· $T^{-1}$] |
| $Q_{10}$ | 10-years recurrence time discharge | [$L^3$· $T^{-1}$] |
| $R_D$ | obstacle Reynolds number | [-] |
| $t$ | time | [T] |
| $t_0$ | initial time | [T] |
| $T$ | uprooting time | [T] |

Continued on next page

**Table A.1 – continued from previous page**

| Symbol | Description | Unit |
|---|---|---|
| $\bar{T}$ | averaged uprooting time | [T] |
| $\hat{t}$ | averaged duration of the flow erosion process | [T] |
| $\widetilde{T}$ | dimensionless time of uprooting | [-] |
| $u$ | flow velocity | [L· T$^{-1}$] |
| $V_f$ | foliage volume | [L$^{-3}$] |
| $V_g$ | sediment volume | [L$^{-3}$] |
| $V_p$ | stem volume | [L$^{-3}$] |
| $V_r$ | root volume | [L$^{-3}$] |
| $V_w$ | water volume | [L$^{3}$] |
| $\dot{\eta}$ | vertical velocity of sediment erosion | [L· T$^{-1}$] |
| $\rho_f$ | foliage density | [M· L$^{-3}$] |
| $\rho_p$ | stem density | [M· L$^{-3}$] |
| $\rho_r$ | root density | [M· L$^{-3}$] |
| $\rho_w$ | water density | [M· L$^{-3}$] |
| $\rho_r^*$ | modified water density | [M· L$^{-3}$] |
| $\sigma_L$ | standard deviation | [L] |
| $\sigma_T$ | standard deviation | [T] |

**Acknowledgments**

I want to express my gratefulness to Sharon Bywater-Reyes for insights, for sharing the dataset and elucidating data analysis. We also thank the Associate Editor, the two anonymous Reviewers, and Alyssa Serlet for constructive and insightful review comments. We do not report any conflicts of interest. All the datasets used in this manuscript can be found under doi:10.17632/td4zyd6zv2.5 and under the supporting information provided by the authors [*Bywater-Reyes et al.*, 2015] and [*Calvani et al.*, 2019].

## References

Aberle, J., and J. Järvelä (2015), Hydrodynamics of vegetated channels, in *Rivers–Physical, Fluvial and Environmental Processes*, pp. 519–541, Springer.

Bailey, P., J. Currey, and A. Fitter (2002), The role of root system architecture and root hairs in promoting anchorage against uprooting forces in allium cepa and root mutants of arabidopsis thaliana, *Journal of Experimental Botany*, *53*, 333–340.

Bankhead, N. L., R. E. Thomas, and A. Simon (2017), A combined field, laboratory and numerical study of the forces applied to, and the potential for removal of, bar top vegetation in a braided river, *Earth Surface Processes and Landforms*, *42*(3), 439–459.

Baptist, M., V. Babovic, J. R. Uthurburu, M. Keijzer, R. Uittenbogaard, A. Mynett, and A. Verwey (2007), On inducing equations for vegetation resistance, *Journal of Hydraulic Research*, *45*(4), 435–450, 10.1080/00221686.2007.9521778.

Bertoldi, W., A. Gurnell, N. Surian, K. Tockner, L. Zanoni, L. Ziliani, and G. Zolezzi (2009), Understanding reference processes: linkages between river flows, sediment dynamics and vegetated landforms along the tagliamento river, italy, *River Research and Applications*, *25*(5), 501–516.

Bertoldi, W., A. Siviglia, S. Tettamanti, M. Toffolon, D. Vetsch, and S. Francalanci (2014), Modelling vegetation controls on fluvial morphological trajectories, *Geophys. Res. Lett.*, *41*.

Bywater-Reyes, S., A. C. Wilcox, J. C. Stella, and A. F. Lightbody (2015), Flow and scour constraints on uprooting of pioneer woody seedlings, *Water Resources Research*, *51*(11), 9190–9206.

Calvani, G., S. Francalanci, and L. Solari (2019), A physical model for the uprooting of flexible vegetation on river bars, *Journal of Geophysical Research: Earth Surface*, *124*(4), 1018–1034.

623 Camporeale, C., E. Perucca, L. Ridolfi, and A. Gurnell (2013), Modeling the interaction be-
624 tween river morphodynamics and riparian vegetation, *Reviews of Geophysics*, *51*, 1–36.
625 Cannon, W. (1949), A tentative classification of root systems, *Ecology*, *30*, 542–548.
626 Caponi, F., and A. Siviglia (2018), Numerical modeling of plant root controls on gravel bed
627 river morphodynamics, *Geophysical Research Letters*, *45*(17), 9013–9023.
628 Church, M. (2006), Bed material transport and the morphology of alluvial river chan-
629 nels, *Annual Review of Earth and Planetary Sciences*, *34*(1), 325–354, 10.1146/an-
630 nurev.earth.33.092203.122721.
631 Connell, B. S., and D. K. Yue (2007), Flapping dynamics of a flag in a uniform stream, *Jour-*
632 *nal of fluid mechanics*, *581*, 33–67.
633 Coutts, M. P. (1983), Root architecture and tree stability, *Plant and Soil*, *71*, 171–188.
634 Crouzy, B., and P. Perona (2012), Biomass selection by floods and related timescales. part 2:
635 Stochastic modeling, *Adv. Water Res.*
636 Doyle, M. W., E. H. Stanley, D. L. Strayer, R. B. Jacobson, and J. C. Schmidt (2005), Ef-
637 fective discharge analysis of ecological processes in streams, *Water Resources Research*,
638 *41*(11), 10.1029/2005WR004222.
639 Edmaier, K. (2014), Uprooting mechansims of juvenile vegetation by flow erosion, Ph.D.
640 thesis, EPFL.
641 Edmaier, K., P. Burlando, and P. Perona (2011), Mechanisms of vegetation uprooting by flow
642 in alluvial non-cohesive sediment, *Hydrology and Earth System Sciences*, *15*, 1615–1627.
643 Edmaier, K., B. Crouzy, P. Burlando, and P. Perona (2012), Experimental characterization of
644 root anchoring in non-cohesive sediment, in *River Flow 2012*.
645 Edmaier, K., B. Crouzy, R. Ennos, P. Burlando, and P. Perona (2014), Influence of root char-
646 acteristics and soil variables on the uprooting mechanics of avena sativa and medicago
647 sativa seedlings, *Earth Surf. Proc. Land.*, *39*, 1354–1364.
648 Edmaier, K., B. Crouzy, and P. Perona (2015), Experimental characterization of vegetation
649 uprooting by flow, *Journal of Geophysical Research: Biogeosciences*, *120*(9), 1812–1824.
650 Edwards, P. J., J. Kollmann, A. M. Gurnell, G. E. Petts, K. Tockner, and J. V. Ward (1999), A
651 conceptual model of vegetation dynamics on gravel bars of a large alpine river, *Wet. Ecol.*
652 *Man.*, *7*, 141–153.
653 Ennos, A., and S. Pellerin (2000), *Root methods: A handbook*, chap. Plant Anchorage, pp.
654 545–565, Springer.

Ennos, A. R. (1989), The mechanics of anchorage in seedlings of sunflower, *helianthus annuus* l., *New Phytologist*, *113*, 185–192.

Ennos, A. R. (1993), The scaling of root anchorage, *Journal of Theoretical Biology*, *161*(1), 61 – 75, DOI: 10.1006/jtbi.1993.1040.

Gregory, P. (2006), *Plant roots, Growth, activity and interaction with soils*, Blackwell Publishing Ltd.

Gregory, P. J., and B. J. Atwell (1991), The fate of carbon in pulse-labelled crops of barley and wheat, *Plant and Soil*, *136*(2), 205–213, 10.1007/BF02150051.

Gurnell, A. (2013), Plants as river system engineers, *Earth Surf. Proc. Land.*, *doi: 10.1002/esp.3397*.

Järvelä, J. (2002), *Determination of flow resistance of vegetated channel banks and floodplains*, pp. 311–318, Swets & Zeitlinger, Lisse.

Johnson, W. C. (2000), Tree recruitment and survival in rivers: Influences of hydrological processes, *Hydrol. Process.*, *14*, 3051–3074.

Karrenberg, S., S. Blaser, J. Kollmann, T. Speck, and P. Edwards (2003), Root anchorage of saplings and cuttings of woody pioneer species in a riparian environment, *Functional Ecology*, *17*, 170–177.

Kiley, D., and R. Schneider (2005), Riparian roots through time, space and disturbance, *Plant and Soil*, *269*, 259–272.

Köstler, J., E. Brückner, and H. Bibelriether (1968), *Die Wurzeln der Waldbäume*, Verlag Paul Parey.

Lake, P., N. Bond, and P. Reich (2007), Linking ecological theory with stream restoration, *Freshwater biology*, *52*(4), 597–615.

Mahoney, J. M., and S. B. Rood (1998), Streamflow requirements for cottonwood seedling recruitment—an integrative model, *Wetlands*, *18*(4), 634–645, 10.1007/BF03161678.

Mickovski, S., A. Bengough, M. Bransby, M. Davies, P. Hallet, and R. Sonnenberg (2007), Material stiffness, branching pattern and soil matric potential affect the pullout of model root systems, *Europ. Journal of Soil Science*, *58*, 1471–1481.

Mickovski, S., P. Hallett, M. Bransby, M. Davies, R. Sonnenberg, and A. Bengough (2009), Mechanical reinforcement of soil by willow roots: impacts of root properties and root failure mechanism in controlled laboratory tests, *Soil Science of America Journal*, *73*, 1276–1285.

Nepf, H. M. (2012), Hydrodynamics of vegetated channels, *Journal of Hydraulic Research*, *50*(3), 262–279.

Oorschot, M. v., M. Kleinhans, G. Geerling, and H. Middelkoop (2016), Distinct patterns of interaction between vegetation and morphodynamics, *Earth Surface Processes and Landforms*, *41*(6), 791–808.

Palmer, M. A., K. L. Hondula, and B. J. Koch (2014), Ecological restoration of streams and rivers: shifting strategies and shifting goals, *Annual Review of Ecology, Evolution, and Systematics*, *45*, 247–269.

Pasquale, N., P. Perona, R. Francis, and P. Burlando (2014), Above-ground and below-ground salix dynamics in response to river processes, *Hydrological Processes*, *28*, 5189–5203.

Perona, P., and B. Crouzy (2018), Resilience of riverbed vegetation to uprooting by flow, *Proc. R. Soc. A*, *474*(2211), 20170,547.

Perona, P., P. Molnar, B. Crouzy, E. Perucca, Z. Jiang, S. McLelland, D. Wüthrich, K. Edmaier, R. Francis, C. Camporeale, and A. Gurnell (2012), Biomass selection by floods and related timescales: Part 1. experimental observations, *Adv. Water Res.*

Pollen, N. (2007), Temporal and spatial variability in root reinforcement of streambanks : Accounting for soil shear strength and moisture, *Catena*, *69*, 197–205, 10.1016/j.catena.2006.05.004.

Pollen, N., and A. Simon (2005), Estimating the mechanical effects of riparian vegetation on stream bank stability using a fiber bundle model, *Water Resouces Research*, *41*, W07,025.

Pollen-Bankhead, N., and A. Simon (2010), Hydrologic and hydraulic effects of riparian root networks on streambank stability: Is mechanical root reinforcement the whole story?, *Geomorphology*, *116*, 353–362.

Schnauder, I., and H. Moggridge (2009), Vegetation and hydraulic-morphological interactions at the individual plant, patch and channel scale, *Aquatic Sciences*, *71*, 318–330.

Schwarz, M., F. Preti, F. Giadrossich, P. Lehmann, and D. Or (2010), Quantifying the role of vegetation in slope stability: A case study in tuscany (italy), *Ecological Engineering*, *36*, 285–291.

Schwarz, M., D. Cohen, and D. Or (2011), Pullout tests of root anchorage and natural bundles in soil: Experiments and modeling, *Journal of Geophysical Research*, *116*, F02,007.

Shields, A. (1936), Anwendung der aehnlichkeitsmechanik und der turbulenzforschung auf die geschiebebewegung, *PhD Thesis Technical University Berlin*.

719 Simon, A., and A. Collison (2002), Quantifying the mechanical and hydrologic effects of
720 riparian vegetation on streambank stability, *Earth Surf. Proc. Land.*, *27*, 527–546.
721 Smit, A. L., A. G. Bengough, C. Engels, M. van Noordwijk, S. Pellerin, and S. C. van de
722 Geijn (2013), *Root methods: a handbook*, Springer Science & Business Media.
723 Tanaka, N., and J. Yagisawa (2009), Effects of tree characteristics and substrate condition on
724 critical breaking moment of trees due to heavy flooding, *Landscape Ecol Eng*, *5*, 59–70.
725 Waisel, Y., and A. Eshel (2002), *Functional diversity of various constituents of a single root*
726 *system, in Plant roots: the hidden half*, Marcel Dekker.
727 Yagci, O., U. Tschiesche, and M. Kabdasli (2010), The role of different forms of natural ri-
728 parian vegetation on turbulence and kinetic energy characteristics, *Advances in water Re-*
729 *sources*, *33*(5), 601–614.
730 Ying, L., G. Jiarong, L. Huipin, Z. Jinrui, and C. Qiang (2011), The root anchorage *ability of*
731 *Salix alba var. tristis* using a pull–out test, *African Journal of Biotechnology*, *10*, 16,501–
732 16,507.
733 Zen, S., G. Zolezzi, M. Toffolon, and A. M. Gurnell (2016), Biomorphodynamic modelling
734 of inner bank advance in migrating meander bends, *Advances in Water Resources*, *93*, 166
735 – 181, https://doi.org/10.1016/j.advwatres.2015.11.017, ecogeomorphological feedbacks
736 of water fluxes, sediment transport and vegetation dynamics in rivers and estuaries.
737 Zong, L., and H. Nepf (2011), Spatial distribution of deposition within a patch of vegetation,
738 *Water Resouces Research*, *47*, W03,516.